IET Circuits, Devices & Systems

Review Article

IET Journals
The Institution of Engineering and Technology

Is graphene a good transparent electrode for photovoltaics and display applications?

ISSN 1751-858X
Received on 8th April 2015
Revised on 18th May 2015
Accepted on 21st May 2015
doi: 10.1049/iet-cds.2015.0121
www.ietdl.org

Thomas H. Bointon, Saverio Russo, Monica Felicia Craciun ✉

Centre for Graphene Science, CEMPS, University of Exeter, Exeter, EX4 4QL, UK
✉ *E-mail: m.f.craciun@exeter.ac.uk*

Abstract: The current standard material used for transparent electrodes in displays, touch screens and solar cells is indium tin oxide (ITO) which has low sheet resistance (10 Ω/□), high optical transmission in the visible wavelength (85%) and does not suffer of optical haze. However, ITO is mechanically rigid and incompatible with future demands for flexible applications. Graphene materials share many of the properties desirable for flexible transparent conductors, including high optical transparency, high mechanical flexibility and strength. Whilst pristine graphene is not a good transparent conductor, functionalised graphene is at least 1000 times a better conductor than its pristine counterpart and it outperforms ITO. Here the authors review recent work on a novel graphene-based conductor with sheet resistance as low as 8.8 Ω/□ and 84% optical transmission. This material is obtained by ferric chloride ($FeCl_3$) intercalation into few-layer-graphene (FLG), giving rise to a new system which is the best known flexible and transparent electricity conductor. $FeCl_3$-FLG shows no significant changes in the electrical and structural properties for a long exposure to air, to high levels of humidity and at temperatures of up to 150°C in atmosphere. These properties position $FeCl_3$-FLG as a viable and attractive replacement to ITO.

1 Introduction

Over the past decades, the landscape of consumer electronics and optoelectronics has changed drastically. Technological advances have led to the development of portable media devices, such as tablets, smart phones and even wearable electronics. At the same time, the development of solar cells has enabled a viable alternative method of producing energy or revolutionary products such as prototypes of solar powered airplanes. However, with all these technological advances also the consumer demands are evolving and new products are under constant development. For example, flexible and more durable mobile phone screens are required as there is the chronic issue of broken displays due to dropping. The current technologies for displays, touch screens and solar cells use indium tin oxide (ITO) as a transparent electrode. However, this material is rigid and flexing or bending ITO causes a significant degradation in its conductive properties. Therefore, future flexible displays and photovoltaics, and the associated electronics require materials that are flexible, optically transparent and electrically conductive.

For a transparent conductor it is vital that the sheet resistance is low. High resistance electrodes have several major issues. First, the resistance of the electrode limits the size of the manufacturable electrode. When using the electrode in a display or solar cell the electrode should have a uniform potential, however, with high resistance electrodes there is a voltage drop as the distance from the contacts connecting the electrode to the rest of the circuit is increased. This leads to a non-uniform voltage potential across the electrode giving non-uniform light emission. To minimise this effect the size of the electrode must be limited. Secondly, the voltage drop across the electrode is dissipated as heat. Heating of the electrode can cause components such as LED pixels to emit more or less light and can reduce the lifetime of the pixels leading to an increase in device faultier rates. Finally, screens are becoming more portable and battery operated as part of high-tech electronics. The dissipation of energy across the electrode increases energy consumption and reduces the battery lifetime of the device. This reduction in the device efficiency limits the range of products that the electrodes can be used in. Similarly for photovoltaics, high resistance electrodes reduces the efficiency of the cells and causes unnecessary thermal heating which also acts to reduce the device lifetime.

ITO, which is the current standard material used for transparent electrodes in displays, touch screens and solar cells, has low sheet resistance (10 Ω/□) while having a high optical transmission (85%) with no optical hazing [1, 2]. However, ITO is mechanically rigid and incompatible with flexible applications [1, 2]. Monolayer and few-layer-graphene (FLG) share many of the properties desirable for flexible transparent conductors, including high optical transparency [3], high mechanical flexibility and strength [4, 5]. However, for graphene materials to fulfil the requirements of transparent conductors they must have similar performance as ITO films. Currently, monolayer graphene has been shown to have high optical transmission (>97%), however, the sheet resistance is typically in excess of 1 kΩ/□. This leads to a higher dissipation of energy in the electrode material, hence reduced device efficiency. To make graphene viable as a transparent conductor it must be functionalised to reduce the sheet resistance while maintaining the high optical transmission. A reduction in the sheet resistance of monolayer and FLG has been achieved through chemical functionalisation, where the best results yield 30 Ω/□ with 90% optical transmission and 125 Ω/□ at 97.7% optical transmission, respectively [4, 6]. However, this is still three times larger than values reported for 10 µm thick ITO [7].

Several types of dopants have been used for the chemical functionalisation of monolayer and FLG, such as gold chloride ($AuCl_3$) [6, 8], ferric chloride ($FeCl_3$) [9–11], nitric acid (HNO_3) [4, 8], thionyl chloride ($SOCl_2$) [12], bis(trifluoromethanesulfonyl) amide (TFSA) [13] and tetracyanoquinodimethane (TCNQ) [14]. Table 1 shows the sheet resistance and optical transmission for different functionalisation of graphene. Among these dopants, $AuCl_3$ was shown to decrease the sheet resistance of monolayer graphene to 150 Ω/□, HNO_3 down to 125 Ω/□ and $FeCl_3$ to 72 Ω/□. However, while decreasing the sheet resistance is one of the most significant aspects for transparent electrodes, other properties such as stability in air, at high temperature and humidity, and resistance to solvents may determine what type of doped graphene is suitable for applications in displays and photovoltaics. Thus, it

Table 1 Sheet resistance and optical transparency for various graphene and graphite based electrodes

Dopant	Material	Thickness	Sheet resistance, Ω/□	Optical transparency at 550 nm, %	Better transparent conductor than ITO
$AuCl_3$	monolayer graphene	1 L	150 [6]	87	no
$AuCl_3$	FLG	2 L	150 [6]	87	no
$AuCl_3$	FLG	4 L	34 [8]	–	no
HNO_3	monolayer graphene	1 L	125 [4]	97.7	no
HNO_3	FLG	2 L	123 [8]	95	no
HNO_3	FLG	3 L	96 [8]	90	no
HNO_3	FLG	4 L	30 [4]	87	no
$FeCl_3$	monolayer graphene	1 L	72 [9]	–	no
$FeCl_3$	FLG	3 L	16 [11]	90	no
$FeCl_3$	FLG	4 L	11 [10]	87	no
$FeCl_3$	FLG	5 L	8 [10]	85	yes
TFSA	monolayer graphene	1 L	129 [13]	85	no
TCNQ	FLG	3 L	140 [14]	88	no
$SOCl_2$	reduced graphene oxide paper	–	103 [12]	82	no
	laser induced graphite	25 μm	17 [16]	–	no

has been reported that HNO_3 and $AuCl_3$ doping of monolayer and FLG is unstable in air, which makes graphene materials functionalised with these dopants not a viable ITO replacement in displays and photovoltaic applications. On the other hand, while $FeCl_3$ doped monolayer graphene is resistant to solvents such as anisole and isopropanol, it is very unstable to humidity due to the reaction of $FeCl_3$ with water [9], which is again undesirable for applications.

Another approach to produce low sheet resistance carbon-based electrodes is to use very thick graphitic layers (see Table 1). Examples include stacking multiple graphene layers [15] or producing graphite films through laser conversion of polymers [16]. Thus the laser induced graphite yields a sheet resistance of 17 Ω/□ for a 25 μm thick film [16]. However, while this method improves the overall resistance of the electrode, it leads to a very low optical transparency. At the same time with such thick layers as electrodes, the device efficiency remains inferior to that of their ITO-based counterparts [15].

Here we review recent work on a novel graphene-based transparent conductor with a sheet resistance as low as 8.8 Ω/□ and 84% optical transmission in the visible wavelength. This material is obtained by intercalation of $FeCl_3$ into FLG. In this case, a strong charge transfer occurs between the graphene- and the intercalant-layers, resulting in heavy p-doping of graphene. This gives rise to a new system which is the best known flexible and transparent material able to conduct electricity. A complementary study of Raman spectroscopy, optical transmission spectroscopy and electrical transport techniques is used to characterise the intercalation of $FeCl_3$ and confirm the suitability of the resulting material as a transparent conductor. Furthermore, a stability study shows that $FeCl_3$-FLG can withstand relative humidity of up to 100% at room temperature for 25 days, as well as temperatures of up to 150°C in air – or as high as 620°C in vacuum as demonstrated by in-situ high resolution transmission electron microscopy measurements. This durability to extreme conditions position $FeCl_3$-FLG as a viable and attractive replacement to ITO in electronics, such as 'smart' mirrors or windows, or even solar panels. Finally, we show that $FeCl_3$-FLG can be employed effectively as a transparent electrode in atomically-thin photodetectors.

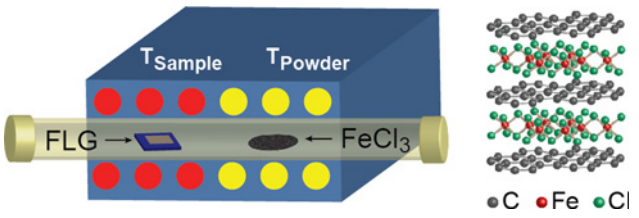

Fig. 1 *Schematic of the two-zone vapour transport method used to intercalate FLG with $FeCl_3$. $FeCl_3$ powder and the substrate with FLG are heated at different temperatures, T_{Powder} and T_{Sample} ($T_{Sample} > T_{Powder}$), in a vacuum sealed glass tube. Schematic crystal structure for $FeCl_3$-FLG is shown on the left*

2 Intercalation of FLG

Intercalation is a process where molecules or atoms can enter at the edges of domains of graphite or FLG structures and then diffuse to form a continuous layer between the graphene sheets [10, 11], see Fig. 1. This process is markedly different from doping of FLG [4, 6, 8, 9, 12–14], where first the monolayers are doped and then sub-sequentially staked to produce the few-layer. Intercalation of various species, such as $FeCl_3$ [10, 11, 19–21], Li [22], K [23, 24], Rb [24], Br [25] and Ca [26], in FLG has been demonstrated so far. The addition of intercalants changes the electrical properties of the FLG. Moreover, there are many other properties that have been reported in intercalated graphite samples. For example, through the intercalation of magnetic molecules such as $FeCl_3$ into graphite inter and intra plane magnetism has been achieved [27], where the magnetic layers in the structure are as thin as 0.5 nm, many times thinner than magnetic films fabricated by thin film deposition techniques [28]. Furthermore, with the intercalation of metals such as lithium and calcium in graphite, there has been an observed superconducting phase transition [29, 30].

The intercalation of graphene structure increases the charge carrier concentration and hence the Fermi energy. This populates higher energy states with charge carriers leading to a higher total number of conducting state, hence to a higher conduction and lower sheet resistance [10]. For example, $FeCl_3$ intercalation has been shown to reduce the sheet resistance of FLG down to 8 Ω/□. More recently, low values of resistivity have also been reported in graphitic lithium intercalated films (sheet resistance of 3 Ω/□ [22]). While the conductivities of the FLG and ultrathin graphite are significantly reduced, these systems have a high optical transmission (above 80%) [10, 22]. In this case, a reduction of the graphite film thickness would improve the optical transmission of the material at the expenses of higher electrical resistivity as expected by Ohm's law. These studies have shown that intercalation is a promising route for tailoring the properties of graphene for the application of transparent conductive electrodes. However, the stability of some intercalated compounds in air, specifically in the presence of moisture and oxygen, is generally poor. For example, it has been reported that lithium intercalated ultrathin graphite is not stable in air and rapidly de-intercalates quickly making the material highly resistive [22]. On the other hand, there are studies demonstrating the stability of $FeCl_3$ doped graphene to a range of solvent environments [9] as well as the extreme stability of $FeCl_3$ intercalated few graphene in high humidity and high temperature in air [31].

The intercalation of few layer graphene with $FeCl_3$ is performed using the two zone vapour transport method [10]. The FLG samples are loaded into a glass tube with anhydrous $FeCl_3$ powder shown in Fig. 1. The tube is evacuated to 1×10^{-5} mbar using a

turbo molecular pump and sealed using an isolation valve. The FLG sample and the $FeCl_3$ powder are placed in two different zones, denoted as T_{Sample} and T_{Powder} which are heated to 360 and 315° C, respectively. The $FeCl_3$ powder sublimes while it is heated, releasing $FeCl_3$ vapour along with a small amount of Cl_2 gas and solid $FeCl_2$. As the $FeCl_3$ vapour passes over the sample it intercalates the FLG. In the final stage of the process T_{Powder} is reduced first to stop the sublimation of $FeCl_3$ and then the rest of the system is cooled.

To make $FeCl_3$ intercalated graphene viable for next generation electrical applications, there are several approaches for producing large area FLG samples (from 1 cm^2 up to few m^2). One approach is to use FLG grown on silicon carbide (4H-SiC) [32]. This method of growth produces high quality films, of size up to 4-inch wafers, with little variation in the number of layers grown and is combined with a substrate which is compatible with the $FeCl_3$ intercalation procedure. Other methods of growing large area FLG to be used for intercalation with $FeCl_3$ involve chemical vapour deposition techniques [33] such as multi-layered graphene grown on nickel and transferred onto a silicon or glass wafer, or multi-layered graphene formed by positioning upon one another a series of monolayer graphene grown on copper. For the experiments discussed in this review, 1 cm^2 epitaxial FLG was obtained through the thermal decomposition of Si face of a 4H-SiC substrate. The C face was cleaned of any graphene present using plasma etching. The sample was then intercalated with $FeCl_3$ for 24 h using the procedure outlined above.

3 Raman spectroscopy of $FeCl_3$ intercalated FLG

Fig. 2*a* shows the Raman spectra for FLG, obtained by mechanical exfoliation on SiO_2/Si, before the intercalation procedure. For the pristine graphene, with increasing the number of layers there is an increase in the G-peak intensity and an evolution of the multi peak structure of the two-dimensional (2D) peak. For the few-layer epitaxial graphene there is a large contribution of the SiC substrate in the spectral region of the G-peak. Fig. 2*c* shows the G and 2D peaks, after subtracting the SiC Raman background. The multi peak structure of the 2D peak indicates that the sample is not monolayer [34]. It has been shown that for FLG grown on SiC the full width at half maximum (FWHM) of the 2D peak exhibits a linear dependence on the inverse number of layers (N): FWHM (2D) = [−45(1/N) + 88] cm^{-1} [17]. The 2D peak of the samples discussed in this review has a FWHM of 72 cm^{-1}, from which a layer number of 3 is estimated.

After the intercalation, for both mechanically exfoliated and epitaxially grown FLG, changes in the Raman spectra are observed due to the charge transfer from the $FeCl_3$ molecules [10, 11, 20, 21]. First an upshift in the position of the G-peak occurs, which is related to the configuration of $FeCl_3$ and the graphene layers in the structure [10, 20, 21], shown in Fig. 3. Specifically, for each layer of graphene which has one adjacent layer of $FeCl_3$ the G-peak is upshifted to 1612 cm^{-1}, known as the G_1 peak. Similarly, for each layer of graphene sandwiched by two $FeCl_3$ layers the G-peak is upshifted to 1624 cm^{-1}, i.e. the G_2 peak. The frequencies, line widths and line shape of the G_1 and G_2 peaks do not depend on the number of graphene layers. The second change in the Raman spectra observed upon $FeCl_3$ intercalation is that the multi-peak structure of the 2D-peak becomes single peaked, as demonstrated in Fig. 3. In addition, in the case of intercalated FLG on SiC the 2D peak position downshifts to that of monolayer graphene on 4H-SiC (2715 cm^{-1}) [17]. The observed changes in the Raman spectra upon intercalation with $FeCl_3$ are consistent with observations from studies where FLG was intercalated with potassium and rubidium [23, 24]. However, in the case of a partial intercalation, identification of the structural composition cannot rely uniquely on the Raman spectra. Further confirmation is required using complementary electrical transport measurements [10].

4 Electrical properties of $FeCl_3$ intercalated FLG

The electrical properties of pristine and $FeCl_3$ intercalated graphene mechanically exfoliated on SiO_2/Si were measured in devices which

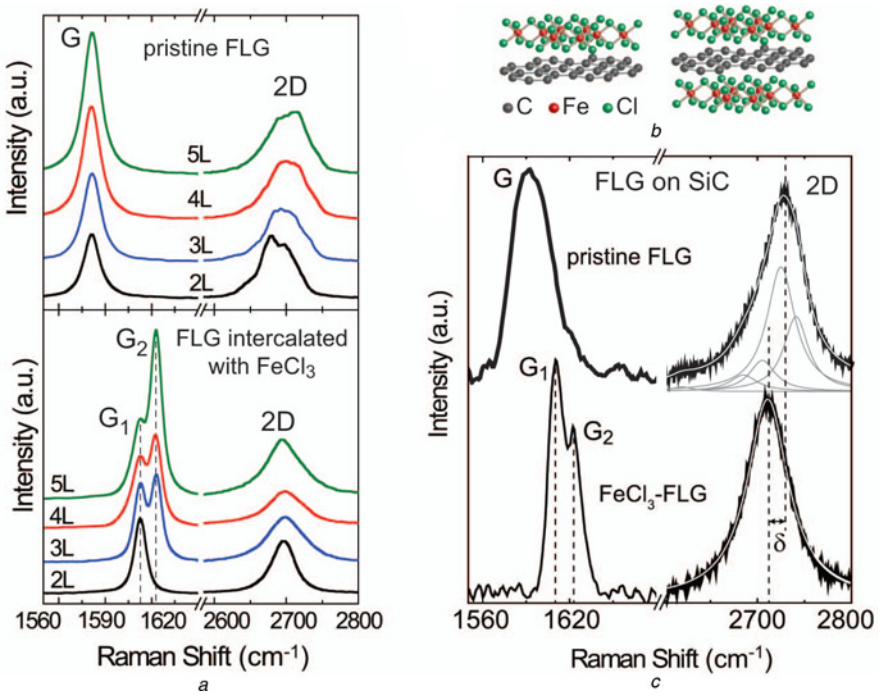

Fig. 2 *Raman spectra of pristine and $FeCl_3$ intercalated FLG*

a G and 2D Raman bands of pristine FLG (top) and of $FeCl_3$-FLG (bottom) with different thicknesses ranging from 2 to 5 L. Reproduced with permission in [10]
b Schematic crystal structure for a graphene sheet with one or two adjacent $FeCl_3$ layers. Reproduced with permission in [10]
c Raman spectra for epitaxial pristine FLG (top) and $FeCl_3$ intercalated FLG (bottom). White curve is a fit of the 2D peak to a multiple Lorentzian function (grey curves). Upon intercalation with $FeCl_3$ a single Lorentzian is the best fit of the 2D peak (white). Reproduced with permission in [11]

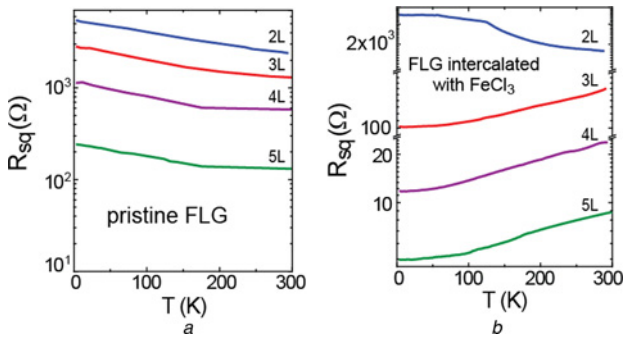

Fig. 3 *Electrical properties of pristine and $FeCl_3$ intercalated graphene mechanically exfoliated on SiO_2/Si*

a Square resistance for pristine FLG of different thicknesses as function of temperature. These devices are fabricated on SiO_2/Si substrates and the highly-doped Si substrate is used as a gate to adjust the Fermi level to the charge neutrality of the system. Reproduced with permission in [10]

b Temperature dependence of the square resistance for $FeCl_3$-FLG of different thicknesses. Reproduced with permission in [10]

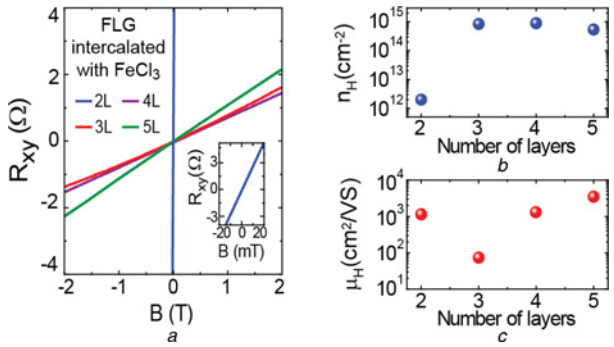

Fig. 5 *Hall coefficient measurements for the estimation of carrier density and mobility of $FeCl_3$-FLG*

a Hall resistance of $FeCl_3$-FLG as a function of magnetic field. Inset shows the data for the bilayer sample on a smaller B scale. Reproduced with permission in [10]

b Carrier density for $FeCl_3$-FLG as a function of the number of graphene layers. Reproduced with permission in [10]

c Carrier mobility for $FeCl_3$-FLG as a function of the number of graphene layers. Reproduced with permission in [10]

were patterned into a Hall bar geometry and electrically contacted with Au/Cr electrodes using electron beam lithography, Ar plasma etching (for patterning), thermal evaporation and lift-off (for Au/Cr). The sheet resistance of the pristine and $FeCl_3$ intercalated epitaxial FLG was measured in a four terminal configuration in macroscopic samples, with a conductive channel of fixed width (0.7 cm) and channel length ranging from 0.7 to 4.2 mm using Ti/Au (5/50 nm) contacts.

The sheet resistance of pristine and $FeCl_3$ intercalated FLG with 2 up to 5 layers was measured as a function of temperature, as shown in Fig. 3*a*. The room temperature sheet resistance of bilayer graphene is as high as 2.5 kΩ/□ and is monotonously decreasing to 120 Ω/□ for five-layer-graphene. Furthermore, a semi-metallic temperature dependence is observed, where the sheet resistance of all of the pristine graphene samples increases with lowering the temperature. On the contrary, the sheet resistance of $FeCl_3$ intercalated FLG, Fig. 3*b*, shows a significant reduction in the room temperature value for all thicknesses. The sheet resistance decreases as the layer number increases reaching a value as low as 8 Ω/□ for five layers $FeCl_3$-FLG. Furthermore, $FeCl_3$-FLG shows the temperature dependence of a metallic conductor, where the resistivity decreases with lowering the temperature. Fig. 4*a* shows that the pristine epitaxial graphene has an average sheet resistance of 174 ± 9 Ω/□, estimated from the linear fit. The corresponding values of resistance in the same devices after intercalation with $FeCl_3$ are systematically lower with an average value of 16.6 ± 0.6 Ω/□. The distribution of sheet resistance of pristine and $FeCl_3$ intercalated epitaxial graphene is presented as two histograms, as shown in Figs. 4*b* and *c*. In both cases, there is a single peaked distribution with narrow spreading of the sheet resistivity demonstrating the homogeneous and reproducible electrical properties in large area $FeCl_3$ intercalated graphene.

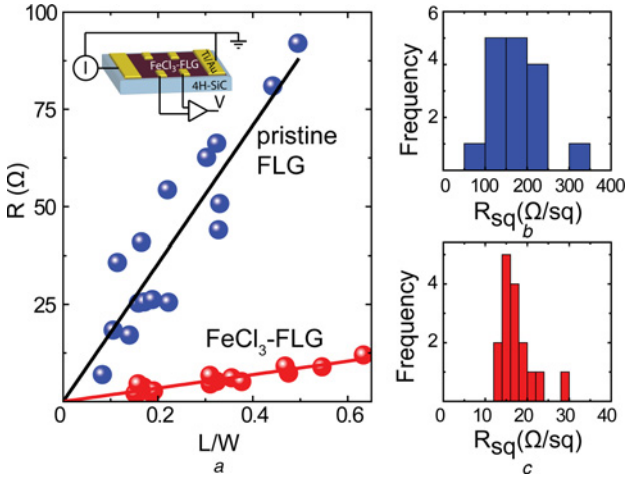

Fig. 4 *Electrical properties of large area pristine and $FeCl_3$ intercalated graphene epitaxially grown on SiC*

a Plot of the measured four terminal resistance (R) as a function of the ratio between the conductive channel length (L) and width (W). Top data points correspond to pristine FLG on 4HSiC while the bottom data points correspond to $FeCl_3$-FLG on 4H-SiC. Inset shows a scheme of the configuration used to measure the resistivity. Reproduced with permission in [11]

b, c Histograms showing the distribution of resistivity for pristine FLG (*b*) and $FeCl_3$-FLG (*c*), respectively. Reproduced with, permission in [11]

To reveal the origin of the low sheet resistance of $FeCl_3$-FLG, the Hall resistance (R_{xy}) was measured as a function of applied perpendicular magnetic field (B), as shown in Fig. 5*a*. Fitting the linear Hall resistance allows for the estimation of the charge carrier concentration (n) using the equation $R_{xy} = V_{xy}/I = -(1/ne)B$ with V_{xy} is the measured Hall voltage, I is the current though the channel and e is the electronic charge. All samples thicker than bilayer have a high charge carrier concentration between 4×10^{14} and 9×10^{14} cm^{-2}, as shown in Fig. 5*b*. For large area epitaxial samples, a concentration of $n > 1.5 \times 10^{14}$ cm^{-2} was achieved. The charge carrier concentration far exceeds the values achievable with top-gates on SiC [18] and is comparable to that achieved in electric double layer FLG transistors [35]. Furthermore, the sign of the fitted gradient shows the dominant charge carriers are holes. This record high charge carrier concentration is three orders of magnitude larger than pristine graphene. The increased charge carrier concentration increases the Fermi energy, hence the increase in the conduction of the material. To demonstrate that there is no degradation of the electrical quality of the intercalated graphene, the charge carrier mobility is estimated, $\mu_H = 1/(n_H e \rho_{xx})$ with ρ_{xx} is the longitudinal resistivity and e is the electron charge, which is shown in Fig. 5*c*. Charge carrier mobilities similar to pristine graphene are observed in the intercalated samples, with a maximum value of 3650 cm^2/(V s). Furthermore, the room temperature mean free path for five-layer-intercalated graphene is 0.6 μm, suggesting low amounts of disorder or structural damage present after the intercalation process.

5 Optical properties of $FeCl_3$ intercalated FLG

The optical properties of $FeCl_3$-FLG were studied in samples with the different number of layers deposited onto the transparent glass substrates. To monitor the change in the optical transmission the measurements were done before and after the intercalation of FLG.

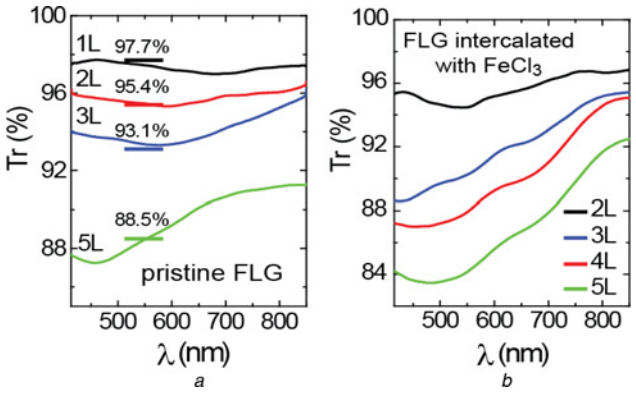

Fig. 6 *Optical properties of $FeCl_3$-FLG*

a Transmittance spectra of pristine FLG. Horizontal lines are the corresponding transmittances at the wavelength of 550 nm reported in the literature. Reproduced with permission in [10]
b Transmittance spectra of $FeCl_3$-FLG. Reproduced with permission in [10]

Fig. 6*a* shows the optical transmission of pristine FLG with the different number of layers while Fig. 6*b* shows the optical transmission after their intercalation with $FeCl_3$, both for the visible wavelength range of light (400–850 nm). Upon intercalation, the transmittance slightly decreases at low wavelengths, but it is still above 80%. In particular for 550 nm, the transmission of pristine FLG ranges from 97.7% for monolayer graphene to 88.5% for five-layer-graphene. The $FeCl_3$ intercalated bilayer graphene has a transmission of 94.5%, which reduces monotonously to 84.1% for five layers. For wavelengths longer than 550 nm we observe an increase in the optical transparency of $FeCl_3$-FLG. This is a significant advantage of $FeCl_3$-FLG material compared to ITO whose transparency decreases for wavelengths longer than 600 nm [2]. This property will provide useful applications that require conductive electrodes which are transparent both in visible and near infrared ranges. For instance, $FeCl_3$-FLG transparent electrodes could be used for solar cells to harvest energy over an extended wavelength range as compared to ITO-based devices.

6 Stability of $FeCl_3$ intercalated FLG

The FLG intercalated with different species such as Li [22], K [23, 24], Rb [24], Br [25] and Ca [26], are not stable upon exposure to air, resulting in their de-intercalation. On the other hand, $FeCl_3$ is highly soluble in water, therefore it would be intuitive to suggest that $FeCl_3$ intercalated graphene would not be stable in air, due to the ambient humidity, quickly reducing the material to pristine graphene. However, it was found that $FeCl_3$-FLG is stable in a variety of conditions and shows no significant de-intercalation [10, 31]. This stability was demonstrated with four experiments: (i) material processing using standard electron beam lithography; (ii) leaving the sample exposed to atmosphere for 1 year and comparing the Raman spectra before and after; (iii) heating the sample in atmosphere up to 150°C and measuring the room temperature resistivity; and (iv) exposing a sample to high levels of humidity (>95%) and measuring the resistivity.

We use Raman spectroscopy to characterise the homogeneity of the $FeCl_3$ intercalation in FLGs after the fabrication of electrical contacts using standard electron beam lithography. During this process, the samples are coated with a Poly(methyl methacrylate) (PMMA) bilayer (495 K PMMA and the second layer is a 950 K PMMA), both are baked at 180°C for 3 min, followed by electron beam writing, development in a solution of Methyl isobutyl ketone-isopropyl alcohol (MIBK-IPA), thermal evaporation for the metallic contacts, lift-off in acetone and rinsing in IPA. Fig. 7*a* shows a micrograph picture of the 5 L intercalated device. A direct comparison of the Raman spectra measured at ten different locations on the device (Fig. 7*b*), as highlighted in the picture, shows no appreciable variation in either intensity or position of the Raman peaks. This demonstrates that the intercalated flakes have a high homogeneity, i.e. the structure is the same at any point of the flake.

Fig. 7*c* shows a comparison between Raman spectra collected at different positions on a $FeCl_3$-FLG sample, after keeping the samples for 3 months and one year in air. The peak positions shape and relative intensities remain the same. If de-intercalation had occurred, an increase in the G peak and subsequent reduction in the G_1 and G_2 peaks should have been occurred. This is not observed allowing to conclude that $FeCl_3$ intercalated graphene is stable in atmosphere at room temperature.

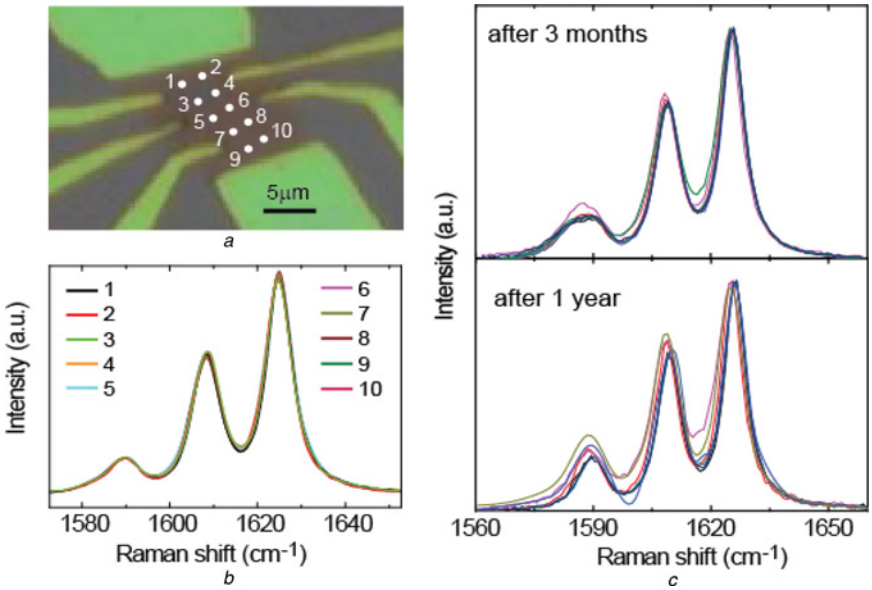

Fig. 7 *Stability of $FeCl_3$-FLG to electron beam lithography fabrication and exposure to air of up to one year*

a Optical image of a $FeCl_3$-FLG device. Reproduced with permission in [10]
b Raman spectra of a $FeCl_3$-FLG devices taken at different locations as indicated in (a). Reproduced with permission in [10]
c Raman spectra of the same $FeCl_3$-FLG device as in b taken at different locations after 3 months and after one year. Reproduced with permission in [10]

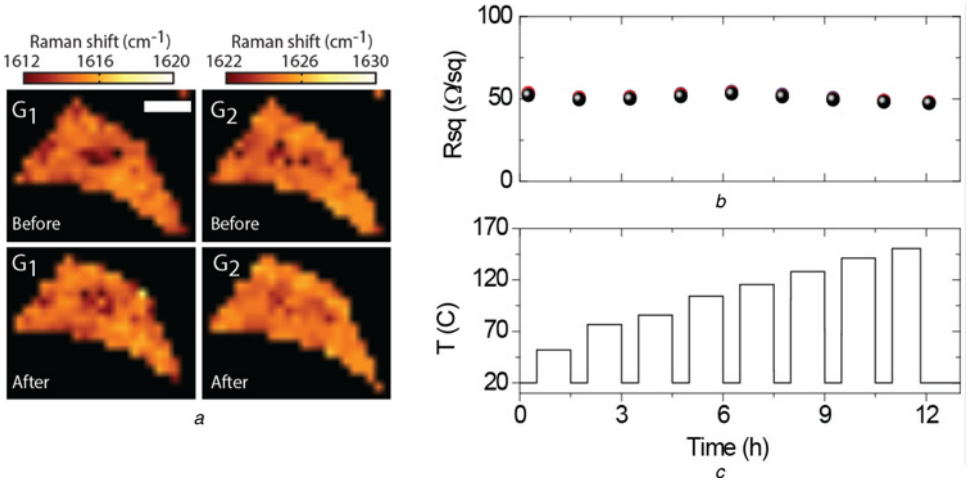

Fig. 8 *Stability of $FeCl_3$-FLG to heating in atmosphere*

a Raman maps showing the G1 and G2 peaks before and after heating to 150°C. Reproduced with permission in [31]
b Sheet resistance measured at room temperature after exposure to heating detailed in (c). Reproduced with permission in [31]

A third experiment was conducted to determine the stability of $FeCl_3$ intercalated graphene up to temperatures of 150°C in atmosphere. The Raman spectra before and after heating are shown in Fig. 8*a*. No changes are observed in the positions of the G_1 and G_2 peaks before and after heating the sample to 150°C for 30 min. This demonstrates that there is no de-intercalation occurring in the sample. Furthermore, the stability at temperatures up to 150°C was tested using electrical transport measurements. For these measurements, the resistivity was first measured at room temperature, the sample was heated to 50°C for 30 min, the sample was cooled to room temperature and the room temperature resistivity was measured. The temperatures the sample was exposed to where incrementally increased from 50 to 150 °C, shown in Fig. 8*b*, with the temperature profile is shown in Fig. 8*c*. As the resistivity of the sample does not change, there is no de-intercalation while the sample is heated in an atmosphere, reinforcing the results from the Raman maps shown in Fig. 8*a*.

Finally, the stability of $FeCl_3$-FLG was demonstrated in high humidity conditions. $FeCl_3$-FLG was loaded into a chamber where the humidity can be controlled from 0 to 95%, and the resistivity was measured in-situ. The resistivity of the sample was measured before humidity exposure, then the sample was exposed to >95% humidity for 1 day. The sample was dried and the resistivity was re-measured. This process was repeated until the cumulative exposure was 24 days. Fig. 9*a* shows the resistivity upon drying the samples against the exposure time to humidity. There was no significant change in the resistivity after the prolonged exposure to high levels of humidity. To complement the electrical transport study for high humidity exposure a Raman study was performed for the same sample. Fig. 9*b* shows the Raman spectra of the same region on the sample after exposure to high levels of humidity. No change is visible in the relative intensities of the G_1 and G_2 peaks after an exposure of 25 days.

Combining the information from the above experiments demonstrates the stability of $FeCl_3$-FLG for long atmospheric exposure, temperatures of up to 150°C and 24 days at >95% humidity.

7 $FeCl_3$ intercalated FLG as a transparent conductor

The high optical transparency observed in $FeCl_3$-FLG is complemented by the remarkable electrical conductivity and outstanding stability to a variety of conditions such as air, humidity and high temperature. However, to replace materials such as ITO as a transparent electrode, the properties should exceed or

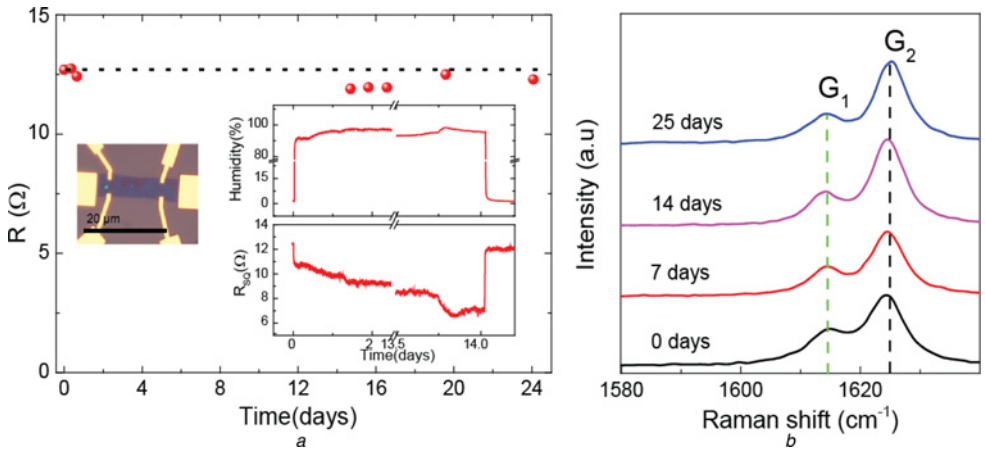

Fig. 9 *Stability of $FeCl_3$-FLG to humidity*

a Sheet resistance of $FeCl_3$-FLG measured after exposure to >95% humidity from 0 to 24 days. Inset picture shows the measured device. Graphs in the inset show the in situ *R*sq against time and the relative levels of humidity. Reproduced with permission in [31]
b Raman spectra for $FeCl_3$-FLG after exposure to humidity (>95%) for 0 to 25 days. Reproduced with permission in [31]

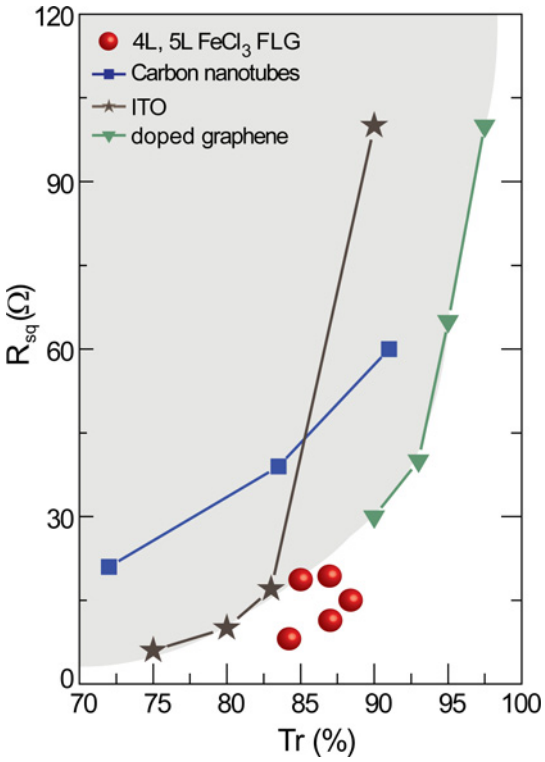

Fig. 10 *Square resistance against transmittance at 550 nm for 4 and 5 L $FeCl_3$-FLG, ITO, carbon-nanotube films and doped graphene materials. $FeCl_3$–FLG outperform the current limit of transparent graphene conductors, which is indicated by the grey area. Reproduced with permission in [10]*

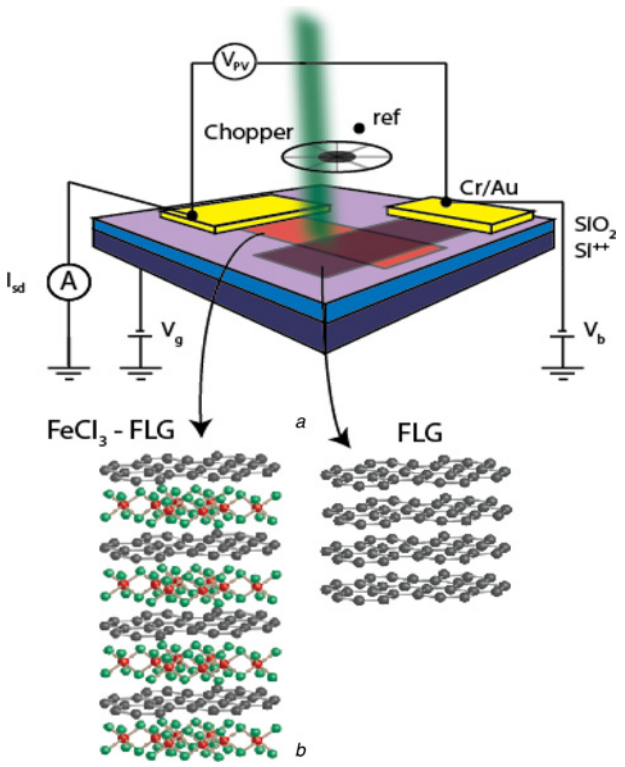

Fig. 11 *Photovoltage spectroscopy for the investigation of graphene/$FeCl_3$-FLG photodetectors. Reproduced with permission in [42]*

a Schematic of the device design and the experimental setup for photovoltage spectroscopy
b Crystal structure for fully intercalated $FeCl_3$-FLG and for FLG flakes

match that of commercially available ITO ($R_s = 10$ Ω/□ with a 550 nm transmission of 85%) [7]. Fig. 10 shows the 550 nm transmission and conductivity of ITO and the leading air-stable carbon-based materials such as doped carbon nanotube arrays [4, 36], doped monolayer graphene and $FeCl_3$-FLG. The multiple points represent different thicknesses of the materials, for example ITO has a resistivity of 7 Ω/□ and 550 nm transmission of 75% for a thick film, where reducing the thickness increases the resistivity to 100 Ω/□ with a 550 nm transmission of 90%. Reducing the material thickness increases the transmission, but reduces the parallel conductance in the film, hence increasing the resistivity, this leads to the bounding grey area highlighting the empirical dependence of resistivity on the 550 nm transmission. In the comparison, the ideal transparent conductor would have a high optical transmission and low resistivity would tend to the bottom right corner of the graph. It is apparent that the resistivity and optical transmission of the five-layer-intercalated graphene outperform the commercially available ITO films. Furthermore, the doped carbon nanotubes and doped monolayer graphene are poor performers, when compared to $FeCl_3$-FLG.

8 Atomically thin photo-detectors using $FeCl_3$ intercalated FLG as transparent electrode

The conversion of photons into electrical signals is of tremendous societal importance since it is used in a multitude of technologies. Photodetectors based on graphene–metal interface [37–41] are at the core of a new generation of ultrafast devices with a remarkable high bandwidth (500 GHz), zero source–drain bias (hence zero dark current) operation, and good internal quantum efficiency. In these devices, photocurrent is generated by illumination of one of the metal/graphene interfaces of a graphene field-effect transistor. However, these devices employ opaque metallic nanostructures which would introduce significant haze caused by light scattering when used in smart windows and mirrors. Therefore, metal electrodes were replaced by $FeCl_3$-FLG [42] to realise an all-graphene-based photodetector. The leap to all-graphene structures which have a high transparency would enable the development of a new generation of transparent photovoltaic devices which do not suffer from haze. In this section, we review the optoelectronic properties of these novel graphene/$FeCl_3$-FLG heterostructures which were investigated using photovoltage spectroscopy.

The graphene/$FeCl_3$-FLG photodetector was fabricated as follows: pristine FLG was first deposited by mechanical exfoliation onto heavily doped Si/SiO_2 substrate and intercalated with $FeCl_3$. Subsequently, a pristine FLG flake was transferred over the $FeCl_3$-FLG flake. Independent multiple electric contacts were made by Cr/Au (5 nm/70 nm) to the bottom $FeCl_3$-FLG and top FLG allowing the characterisation of these heterostructures. Fig. 11 shows the schematic of the final device along with the measurement setup. The $FeCl_3$-FLG flake was kept on the ground, while a small dc bias of 0.1 mV was applied to the pristine FLG flake. The graphene photodetector was then illuminated by a 532 nm HeNe laser focused by using a 100× objective to 1.5 μm spot size at a power of 8.2 μW. The beam was chopped at 370 Hz, and the chopper was used as reference to a lock-in amplifier which measures the photovoltage. The heavily doped Si substrate acts as a global back-gate which was used to tune the chemical potential of graphene, whereas the resistivity of the $FeCl_3$-FLG flake was unaffected by the typical values of used gate voltage due to the high doping level. The devices were mounted on a scanning stage, which allows the mapping of the photoresponse of these graphene-based heterointerfaces in the x–y directions with a spatial resolution of 1 μm. The optoelectronic properties of these graphene-based hybrid structures are characterised by measuring the photovoltage generated across the pristine FLG/$FeCl_3$-FLG interface while rastering the laser spot over the active device area.

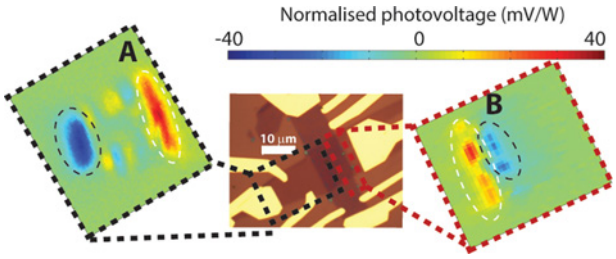

Fig. 12 *Photovoltage spectroscopy for the interfaces of the device highlighted in the optical micrograph picture*

These measurements are taken for the $V_g = 0$ V, 1×10^{-4} V source–drain bias and with a laser power of 8.2 μW. The region highlighted in white in the photovoltage maps corresponds to the FLG/FeCl3-FLG interface and has positive sign, whereas the region highlighted in black is the Au/FLG interface and is negative. In these measurements, the Au contact connected to the FeCl3-FLG flake is grounded while the Au contact connected to the FLG is the source. Reproduced with permission in [42]

Fig. 12 shows the photovoltage generated in a typical device as a function of position of the laser beam. It is apparent that there is a strong photovoltage at the Au/FLG (blue) and FLG/$FeCl_3$-FLG (red) interfaces, while the photovoltage at the $FeCl_3$-FLG/Au is nearly 0.

To understand the origin of the generated photovoltage, the position of the laser beam was fixed on a specific location of the interfaces, and by changing the back-gate voltage, the chemical potential was modulated from holes to electrons in the pristine FLG. Figs. 13*a* and *b* show the gate dependence of the resistance for the different interfaces found in the device as indicated in the graph. In particular, for the pristine flake, the charge neutrality point occurs at 20 V and the crossover from hole transport to electron transport can be studied.

A comparison of the gate dependence (in the range of $-50\ \text{V} < V_g < 70\ \text{V}$) of the photovoltage for all interfaces shows striking differences in the measured signal depending on the interface that is measured (see Figs. 13*c* and *d*). More specifically, no detectable photovoltage was generated at the Au/$FeCl_3$-FLG (black). This is in contrast to the photovoltage generated at the Au/FLG (blue) and FLG/$FeCl_3$-FLG (red) which is non-zero [up to (30 mV/W], it is non-monotonous, it switches sign when the gate voltage drives the Fermi energy across the charge neutrality point, and it decreases monotonously for very high doping levels. The origin of the photovoltage was attributed to photothermoelectric effects. Furthermore, the photovoltage generated at the Au/FLG is of comparable magnitude to that measured at the FLG/$FeCl_3$-FLG interface, but it has opposite sign, that is, negative in the hole side and positive in the electron side. These experiments show that $FeCl_3$-FLG can be used as a replacement for metal contacts in a new generation of all-graphene-based photodetectors.

9 $FeCl_3$ intercalated FLG for flexible applications

The low temperature required for the $FeCl_3$ intercalation process (360°C) allows the use of a wide range of substrates such as glass, Si/SiO_2, SiC, as well as flexible substrates which are compatible with existing flexible technologies. Examples of high temperature resistant flexible substrate include Kapton® PV9100 series polyimide films [43] which are flexible substrates for thin film photovoltaic technologies and have been successfully used in applications at temperatures as high as 400° C. On the other hand, several methods developed for the dry transfer of graphene on arbitrary substrates [4, 44–47] can be employed to transfer $FeCl_3$-FLG from glass, Si/SiO_2 or SiC onto flexible substrates that do not tolerate the conditions of the intercalation process, such as polyethylene terephthalate, polyethylene naphthalate (PEN) and polymers. In particular, Caldwell *et al.* [44] demonstrated the dry transfer of epitaxial graphene from SiC onto arbitrary substrates using thermal release tape. Using the thermal release tape method we have transferred $FeCl_3$-FLG from a glass to a flexible PEN substrate, see Fig. 14a. To demonstrate the conduction of the transferred film the sample was tested as a component in a simple circuit. Contacts were attached to the sample using silver paint and put in series with a battery and an LED. Fig. 14*b* demonstrates the transferred film conducting while the substrate is deformed by flexing.

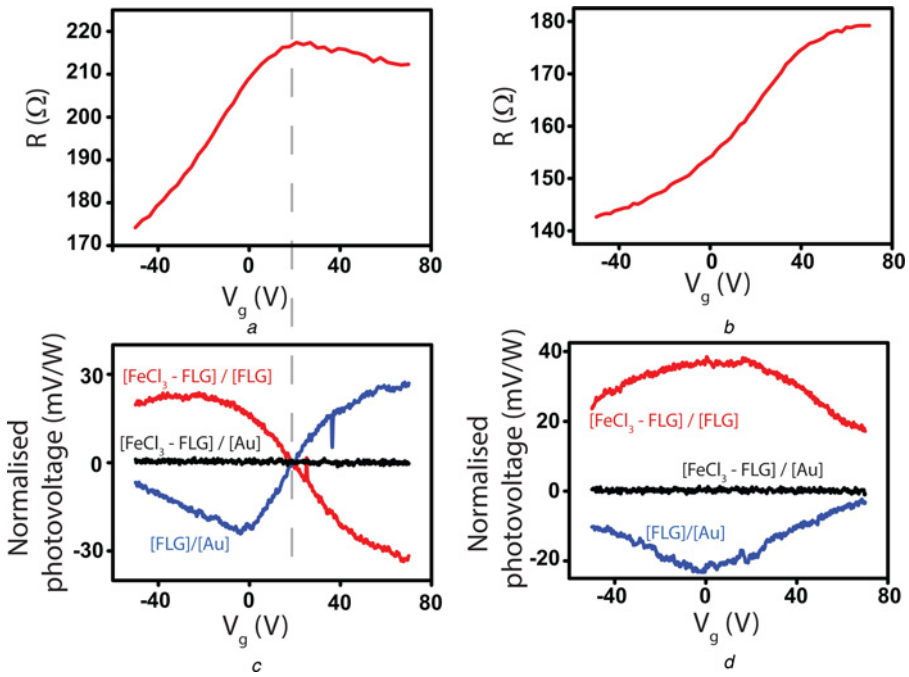

Fig. 13 *Gate tunable photovoltage in graphene/$FeCl_3$-FLG photodetectors. Reproduced with permission in [42]*

a Gate dependence of the resistance for interface A
b Gate dependence of the resistance for interface B
c Gate dependence of the photovoltage when the laser position is located at the Au/$FeCl_3$-FLG (top left and bottom right), FLG/$FeCl_3$-FLG (middle) and the $FeCl_3$-FLG/Au (bottom left and top right) for interface A
d Gate dependence of the photovoltage when the laser position is located at the Au/$FeCl_3$-FLG (top), FLG/$FeCl_3$-FLG (middle), and the $FeCl_3$-FLG/Au (bottom) for interface B

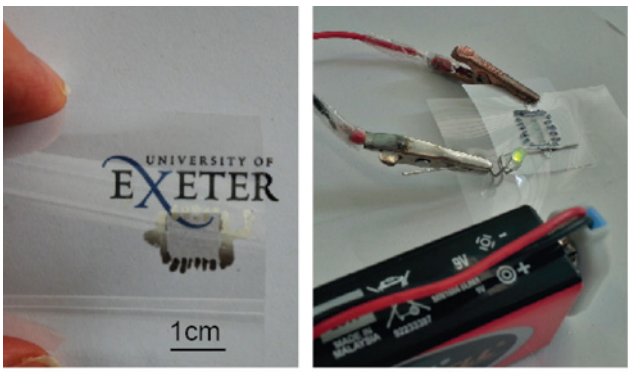

a b

Fig. 14 *$FeCl_3$-FLG transferred from glass to a PEN substrate*

a Photograph of $FeCl_3$-FLG on flexible and transparent PEN substrate
b Photograph demonstrating the $FeCl_3$-FLG conducting while the substrate is flexed

10 Conclusions

Graphene materials have great potential for future electronic devices with novel functionalities due to their tuneable properties [48–53], as well as for emerging flexible and wearable technologies [54] such as healthcare electronics and energy-harvesting devices. Recent advances in chemical functionalisation have shown that the properties of graphene materials can even be enhanced to unprecedented levels by chemical bonding of a molecule or a chemical element to the pristine material [55–58]. The most recent example of the potential of chemical functionalisation is FLG intercalated with $FeCl_3$ dubbed GraphExeter [59]. In this case, functionalisation with $FeCl_3$ of FLG results in the best transparent electrical conductor which outperforms indium–tin oxide used currently in displays.

In this paper, we have reviewed recent work on the successful functionalisation of FLG through $FeCl_3$ intercalation [10, 11, 33, 60, 61] which is confirmed though Raman spectroscopy and electrical transport measurements. Through intercalation, a significant reduction of the electrical resistivity of up to three orders of magnitude is achieved when $FeCl_3$-FLG is compared to the pristine analogue. Only small changes occur in the high optical transmission spectra of FLG after the intercalation procedure, where the optical transmission is still high enough to compete with commercially used ITO films. A systematic study of the stability of $FeCl_3$-FLG shows no significant changes in the electrical and structural properties for a long exposures to air, to high levels of humidity and at temperatures of up to 150°C in atmosphere. Finally, the investigation of novel graphene/$FeCl_3$-FLG heterostructures demonstrated that $FeCl_3$-FLG can replace metals in a new generation of all-graphene photodetectors [42, 62]. The technological advantages combined with the unique electro-optical properties found in $FeCl_3$-FLG make these materials a valuable alternative to ITO for photovoltaics and display applications.

11 Acknowledgments

S.R. and M.F.C acknowledge financial support from EPSRC (grant no. EP/J000396/1, EP/K017160/1, EP/K010050/1, EPG036101/1, EP/M001024/1, EPM002438/1) and from Royal Society international Exchanges Scheme 2012/R3 and 2013/R2.

12 References

1 Kumar, A., Zhou, C.: 'The race to replace tin-doped indium oxide: which material will win?', *ACS Nano*, 2010, **4**, (1), pp. 11–14
2 Hecht, D.S., Hu, L., Irvin, G.: 'Emerging transparent electrodes based on thin films of carbon nanotubes, graphene, and metallic nanostructures', *Adv. Mater.*, 2011, **23**, (13), pp. 1482–1513
3 Nair, R.R., Blake, P., Grigorenko, A.N., *et al.*: 'Fine structure constant defines visual transparency of graphene', *Science*, 2008, **320**, (5881), p. 1308
4 Bae, S., Kim, H., Lee, Y., *et al.*: 'Roll-to-roll production of 30-inch graphene films for transparent electrodes', *Nat. Nanotechnol.*, 2010, **5**, pp. 574–578
5 Lee, C.C., Wei1, X., Kysar, J.W., *et al.*: 'Measurement of the elastic properties and intrinsic strength of monolayer graphene', *Science*, 2008, **321**, (5887), pp. 385–388
6 Kim, K.K., Reina, A., Shi, Y., *et al.*: 'Enhancing the conductivity of transparent graphene films via doping', *Nanotechnology*, 2010, **21**, (28), pp. 285205–285211
7 De, S., Coleman, J.N.: 'Are there fundamental limitations on the sheet resistance and transmittance of thin graphene films?', *ACS Nano*, 2010, **4**, (5), pp. 2713–2720
8 Han, T.H., Lee, Y., Choi, M.R., *et al.*: 'Extremely efficient flexible organic light-emitting diodes with modified graphene anode', *Nat. Photonics*, 2012, **6**, pp. 105–110
9 Song, Y., Fang, W., Hsu, A.L., *et al.*: 'Iron (III) chloride doping of CVD graphene', *Nanotechnology*, 2014, **25**, p. 395701
10 Khrapach, I., Withers, F., Bointon, T.H., *et al.*: 'Novel highly conductive and transparent graphene-based conductors', *Adv. Mater.*, 2012, **24**, pp. 2844–2849
11 Bointon, T.H., Khrapach, I., Yakimova, R., *et al.*: 'Approaching magnetic ordering in graphene materials by $FeCl_3$ intercalation', *Nano Lett.*, 2014, **14**, (4), pp. 1751–1755
12 Wassei, J.K., Cha, K.C., Tung, V.C., *et al.*: 'The effects of thionyl chloride on the properties of graphene and graphene–carbon nanotube composites', *J. Mater. Chem.*, 2011, **21**, p. 3391
13 Tongay, S., Berke, K., Lemaitre, M., *et al.*: 'Stable hole doping of graphene for low electrical resistance and high optical transparency', *Nanotechnology*, 2011, **22**, p. 425701
14 Hsu, C.L., Lin, C.T., Huang, J.H., *et al.*: 'Layer-by-layer graphene/TCNQ stacked films as conducting anodes for organic solar cells', *ACS Nano*, 2012, **6**, (6), pp. 5031–5039
15 Park, H., Howden, R.M., Barr, M.C., *et al.*: 'Organic solar cells with graphene electrodes and vapor printed poly(3,4-ethylenedioxythiophene) as the hole transporting layers', *ACS Nano*, 2012, **6**, (7), pp. 6370–6377
16 Lin, J., Peng, Z., Liu, Y., *et al.*: 'Laser-induced porous graphene films from commercial polymers', *Nat. Commun.*, 2014, **5**, p. 5714
17 Lee, D.S., Riedl, C., Krauss, B., *et al.*: 'Raman spectra of epitaxial graphene on SiC and of epitaxial graphene transferred to SiO_2', *Nano Lett.*, 2008, **8**, p. 4320
18 Wu, Y., Ye, P.D., Capano, M.A., *et al.*: 'Top-gated graphene field-effect-transistors formed by decomposition of SiC', *Appl. Phys. Lett.*, 2008, **92**, p. 092102
19 Kim, N., Kim, K.S., Jung, N., *et al.*: 'Synthesis and electrical characterization of magnetic bilayer graphene intercalate', *Nano Lett.*, 2011, **11**, pp. 860–865
20 Zhao, W.P., Tan, H., Liu, J., *et al.*: 'Intercalation of few-layer graphite flakes with $FeCl_3$: Raman determination of Fermi level, layer by layer decoupling, and stability', *J. Am. Chem. Soc.*, 2011, **133**, p. 5941
21 Zhan, D., Sun, L., Ni, Z.H., *et al.*: '$FeCl_3$-based few-layer graphene intercalation compounds: single linear dispersion electronic band structure and strong charge transfer doping', *Adv. Func. Mater.*, 2010, **20**, p. 3504
22 Boa, W., Wan, J., Han, X., *et al.*: 'Approaching the limits of transparency and conductivity in graphitic materials through lithium intercalation', *Nat. Commun.*, 2014, **5**, p. 4224
23 Howard, C.A., Dean, M.P.M., Withers, F.: 'Phonons in potassium-doped graphene: the effects of electron-phonon interactions, dimensionality, and adatom ordering', *Phys. Rev. B*, 2011, **84**, p. 241404 (R)
24 Jung, N., Kim, B., Crowther, A.C., *et al.*: 'optical reflectivity and Raman scattering in few-layer-thick graphene highly doped by K and Rb', *ACS Nano*, 2011, **5**, p. 5708
25 Hwang, J., Carbotte, J.P., Tongay, S., *et al.*: 'Ultrapure multilayer graphene in bromine-intercalated graphite', *Phys. Rev. B*, 2011, **84**, p. 041410
26 Kanetani, K., Sugawara, K., Sato, T., *et al.*: 'Ca intercalated bilayer graphene as a thinnest limit of superconducting C_6Ca', *PNAS*, 2012, **109**, pp. 19610–19613
27 Dresselhaus, M.S., Dresselhaus, G.: 'Intercalation compounds of graphite', *Adv. Phys.*, 1981, **30**, pp. 139–326
28 Bader, S.D.: 'Thin film magnetism', *Proc. IEEE*, 1990, **78**, pp. 909–922
29 Weller, T.E., Ellerby, M., Saxena, S.S., *et al.*: 'Superconductivity in the intercalated graphite compounds C_6Yb and C_6Ca', *Nat. Phys.*, 2005, **1**, pp. 39–41
30 Pan, Z.H., Camacho, J., Upton, M.H., *et al.*: 'Electronic structure of superconducting KC8 and nonsuperconducting LiC_6 graphite intercalation compounds: evidence for a graphene-sheet-driven superconducting state', *Phys. Rev. Lett.*, 2011, **106**, p. 187002
31 Wehenkel, D.J., Bointon, T.H., Booth, T., *et al.*: 'Unforeseen high temperature and humidity stability of $FeCl_3$ intercalated few layer graphene', *Sci. Rep.*, 2015, **5**, p. 7609
32 Eriksson, J., Pearce, R., Iakimovet, T., *et al.*: 'The influence of substrate morphology on thickness uniformity and unintentional doping of epitaxial graphene on SiC', *Appl. Phys. Lett.*, 2012, **100**, p. 241607
33 Russo, S., Craciun, M.F., Bointon, T.H.: 'Doped graphene'. International Patent WO2015049490 (A1), April 2015
34 Ferrari, A.C., Meyer, J.C., Scardaci, V., *et al.*: 'Raman spectrum of graphene and graphene layers', *Phys. Rev. Lett.*, 2006, **97**, p. 187401
35 Uesugi, E., Goto, H., Eguchi, R., *et al.*: 'Electric double-layer capacitance between an ionic liquid and few layer graphene', *Sci. Rep.*, 2013, **3**, p. 1595
36 Hecht, D.S., Heintz, A.M., Lee, R., *et al.*: 'High conductivity transparent carbon nanotube films deposited from superacid', *Nanotechnology*, 2011, **22**, p. 075201
37 Surajit, G., Biddut, K.S., Anindarupa, C., *et al.*: 'Position dependent photodetector from large area reduced graphene oxide thin films', *Appl. Phys. Lett.*, 2010, **96**, p. 163109
38 Park, J., Ahn, Y.H., Ruiz-Vargas, C.: 'Imaging of photocurrent generation and collection in single layer graphene', *Nano Lett.*, 2009, **9**, pp. 1742–1746
39 Xia, F., Mueller, T., Lin, Y., *et al.*: 'Ultrafast graphene photodetector', *Nat. Nanotechnol.*, 2009, **4**, pp. 839–843
40 Mueller, T., Xia, F., Avouris, P.: 'Graphene photodetectors for high-speed optical communications', *Nat. Photonics*, 2010, **4**, pp. 297–301

41 Nazin, G., Zhang, Y., Zhang, L., *et al.*: 'Visualization of charge transport through Landau levels in graphene', *Nat. Phys.*, 2010, **6**, pp. 870–874
42 Withers, F., Bointon, T.H., Craciun, M.F., *et al.*: 'All-graphene photodetectors', *ACS Nano*, 2013, **7**, (6), pp. 5052–5057
43 'Kapton® PV9100 Series – Du Pont products' http://www.dupont.com/products-and-services/membranes-films/polyimide-films/brands/kapton-polyimide-film/products/kapton-pv9100-series.html, accessed 12 May 2015
44 Caldwell, J.D., Anderson, T.J., Culbertson, J.C., *et al.*: 'Technique for the dry transfer of epitaxial graphene onto arbitrary substrates', *ACS Nano*, 2010, **4**, (2), pp. 1108–1114
45 Lock, E.H., Baraket, M., Laskoski, M., *et al.*: 'High-quality uniform dry transfer of graphene to polymers', *Nano Lett.*, 2012, **12**, pp. 102–107
46 Fechine, G.J.M., Martin-Fernandez, I., Yiapanis, G., *et al.*: 'Direct dry transfer of chemical vapor deposition graphene to polymeric substrates', *Carbon*, 2015, **83**, pp. 224–231
47 Jung, W., Kim, D., Lee, M., *et al.*: 'Ultraconformal contact transfer of monolayer graphene on metal to various substrates', *Adv. Mater.*, 2014, **26**, pp. 6394–6400
48 Craciun, M.F., Russo, S., Yamamoto, M., *et al.*: 'Tuneable electronic properties in graphene', *Nano Today*, 2011, **6**, pp. 42–60
49 Jhang, S.H., Craciun, M.F., Schmidmeier, S., *et al.*: 'Stacking-order dependent transport properties of trilayer graphene', *Phys. Rev. B, Rapid Commun.*, 2011, **84**, pp. 161408–161412
50 Craciun, M.F., Russo, S., Yamamoto, M., *et al.*: 'Trilayer graphene is a semimetal with a gate-tunable band overlap', *Nat. Nanotechnol.*, 2009, **4**, pp. 383–388
51 Shioya, H., Craciun, M.F., Russo, S., *et al.*: 'Straining graphene using thin film shrinkage methods', *Nano Lett.*, 2014, **14**, pp. 1158–1163
52 Khodkov, T., Withers, F., Hudson, D.C., *et al.*: 'Electrical transport in suspended and double gated trilayer graphene', *Appl. Phys. Lett.*, 2012, **100**, pp. 013114–013117
53 Shioya, H., Yamamoto, M., Russo, S., *et al.*: 'Gate tunable non-linear currents in bilayer graphene diodes', *Appl. Phys. Lett.*, 2012, **100**, pp. 033113–033117
54 Neves, A.I.S., Bointon, T.H., Melo, L.V., *et al.*: 'Transparent conductive graphene textile fibers', *Sci. Rep.*, 2015, **5**, p. 9866
55 Craciun, M.F., Khrapach, I., Barnes, M.D., *et al.*: 'Properties and applications of chemically functionalized graphene', *J. Phys. Condens. Matter*, 2013, **25**, p. 423201
56 Martins, S.E., Withers, F., Dubois, M., *et al.*: 'Tuning the transport gap of functionalized graphene via electron beam irradiation', *New J. Phys.*, 2013, **15**, p. 033024
57 Withers, F., Bointon, T.H., Dubois, M., *et al.*: 'Nanopatterning of fluorinated graphene by electron beam irradiation', *Nano Lett.*, 2011, **11**, pp. 3912–3916
58 Withers, F., Russo, S., Dubois, M., *et al.*: 'Tuning the electronic transport properties of graphene through functionalisation with fluorine', *Nanoscale Res. Lett.*, 2011, **6**, p. 526
59 'GraphExeter-University of Exeter' http://www.exeter.ac.uk/business/ip/commercial/graphexeter/, accessed 12 May 2015
60 Russo, S., Craciun, M.F.: 'Graphene-based material'. Korean Patent KR20140095614 (A), August 2014
61 Russo, S., Craciun, M.F.: 'Graphene-based material'. US Patent US2014174513 (A1), June 2014
62 Withers, F., Bointon, T.H., Craciun, M.F., *et al.*: 'Detector'. International Patent WO2014111702 (A2), July 2014